Energy Shaping Methods for Asymptotic Force Regulation of Compliant Mechanical Systems

David Navarro-Alarcon, *Student Member, IEEE*, Yun-Hui Liu, *Fellow, IEEE*, Jose Guadalupe Romero, and Peng Li

***Abstract*— In this brief, we address the robust force regulation problem of mechanical systems in physical interaction with compliant environments. The control method that we present is entirely derived under the energy shaping framework. Note that for compliant interactions, standard energy shaping methods (i.e., potential shaping controls using static-state feedback actions) cannot guarantee asymptotic stability since they are not robust to unmodeled forces. To cope with this issue, in this brief, we integrate force sensory feedback with a robust energy shaping design. This methodology allows us to incorporate integral force controls while preserving in closed loop the port-Hamiltonian structure, something that is not possible with traditional force regulators. We discuss the practical implementation of our method and provide simple numerical algorithms to compute in real time some of its control terms. To validate our approach, we report an experimental study with an open architecture robot manipulator.**

***Index Terms*— Force regulation, Hamiltonian mechanics, Lyapunov stability, passivity-based control, robot manipulators.**

I. Introduction

THE compliant force regulation problem arises in applications where a controllable mechanical system (typically a robot manipulator) needs to exert a desired force profile onto a deformable environment. It is used in economically important areas, such as surgical robotics [1], and is becoming highly valued as robots migrate from industrial settings to the unstructured human environments [2]. Note that many of the applications of this problem involve contact with deformable materials whose exact stiffness properties are rarely known beforehand.

To guarantee the safety of these contact tasks (which is a major issue in applications involving humans), an energetically passive interaction between the mechanism and the deformable environment is needed. However, the main difficulty to preserve this passive behavior while simultaneously controlling the applied force comes from the unknown potential energy that is induced to the mechanical system by the compliant environment. This unknown potential makes standard energy shaping methods [3] (i.e., static-state feedback controls) unsuitable, since they are not robust to unmodeled forces. This issue is traditionally tackled by adding a simple integral action of the error to be minimized; however, it is well known that the trivial definition of this integrator makes difficult[1] to guarantee closed-loop passivity [4].

In this brief, we address the asymptotic force regulation problem from an energy shaping perspective [5]. The control method that we present is entirely derived under the port-Hamiltonian framework [6], and formulated for torque-controlled mechanical systems in physical interaction with purely elastic (i.e., lossless) environments.

A. Related Work

Note that most of the energy shaping approaches for explicit force regulation are formulated for rigid contact [7]–[11]. For compliant interactions, some of the earliest works to consider the environment's potential energy are due to [12] and [13]. The so-called force/position parallel control scheme is proposed in [14]. This approach is based on a simple PI force regulator, and its stability is proved with traditional Lyapunov theory.[2] However, the simplicity of the control law leads to restrictive conditions on feedback gains that must be satisfied to ensure stability. A method to select these gains is presented in [15]. Doulgeri and Karayiannidis [16] report a force regulator with an adaptive control component; similar to [14], the stability of this controller depends on conditions of several feedback gains. Compliant force regulation is formulated in [17] as an impedance matching problem [18] for mechanical circuits. This passivity-based approach ensures asymptotic stability of the contact force error; however, it only formulates the problem for a simple 1-D contact force.

The enforcement of robust asymptotic stability while preserving in closed loop some sort of port-Hamiltonian structure (i.e., a skew-symmetric matrix representing gyroscopic effects, along with a positive symmetric matrix representing energy dissipation [5]) remains an open problem. Note that none of the above-mentioned approaches address this issue; the classical impedance control [18] can be framed within this formalism, but it is not straightforward to add force

Manuscript received October 7, 2013; accepted February 22, 2014. Manuscript received in final form March 2, 2014. Date of publication March 20, 2014; date of current version October 15, 2014. This work was supported in part by Hong Kong RGC under Grant 415011 and Grant CUHK6/CRF/13G, in part by the Hong Kong ITF under Grant ITS/475/09, and in part by the Shun Hing Institute of Advanced Engineering, Chinese University of Hong Kong. Recommended by Associate Editor M. Zefran.

D. Navarro-Alarcon and P. Li are with the Department of Mechanical and Automation Engineering, The Chinese University of Hong Kong, Hong Kong (e-mail: dnavarro@mae.cuhk.edu.hk; pli@mae.cuhk.edu.hk).

Y.-H. Liu is with the Department of Mechanical and Automation Engineering, The Chinese University of Hong Kong, Hong Kong, and is also visiting the State Key Laboratory on Robotics and Systems, Harbin Institute of Technology, Harbin 150001, China (e-mail: yhliu@mae.cuhk.edu.hk).

J. G. Romero is with SUPELEC, Gif-sur-Yvette 91192, France (e-mail: romerovelazquez@lss.supelec.fr).

Color versions of one or more of the figures in this paper are available online at http://ieeexplore.ieee.org.

Digital Object Identifier 10.1109/TCST.2014.2309659

[1] That is, several feedback gain and initial error conditions must be simultaneously satisfied.

[2] Note that for these types of controllers, the closed-loop Lyapunov function must be properly chosen to prove stability, something that is not needed with the energy shaping methods that we propose in this brief.

controls. Recently, various researchers have tackled this challenging control design problem, e.g., a method to include integral controls for a class of port-Hamiltonian dynamics is proposed in [19] and [20]. For the case of mechanical systems, [21] reports a method to incorporate passive integral actions through a suitable change of momenta coordinates. The tracking problem for port-Hamiltonian dynamics is tackled through time-dependent canonical coordinate transformations in [22]. However, none of these Hamiltonian control approaches address the compliant force regulation problem; our aim in this brief is precisely to fill this gap in the literature.

B. Contribution of This Brief

To contribute to this problem, in this brief, we present an energy shaping force controller that arises from robustifying the static-state feedback regulator in [23] with the robust energy shaping design in [21]. Note that our method is entirely derived within the port-Hamiltonian framework, therefore its closed-loop Lyapunov function is uniquely constructed with the presented methodology—this feature clearly contrasts with traditional PI regulators. To enforce asymptotic stability, our new regulator incorporates nonlinear integral force controls that preserve in closed-loop the port-Hamiltonian structure. To facilitate the control implementation, we provide numerical algorithms that compute in real time (RT) the controller. We report an experimental study to validate this method.

C. Organization

The rest of this brief is organized as follows. Section II presents the mathematical modeling. Sections III and IV derive the controller. Section V reports the experiments. Section VI gives the conclusion.

II. Mathematical Modeling

A. Notation

We denote column vectors and matrices by small and capital bold letters, e.g., $\mathbf{z} \in \mathbb{R}^h$ and $\mathbf{Z} \in \mathbb{R}^{g\times h}$. We denote the identity and null matrices by $\mathbf{I}_{h\times h} \in \mathbb{R}^{h\times h}$ and $\mathbf{0}_{h\times g} \in \mathbb{R}^{h\times g}$, respectively, and the null vector by $\mathbf{0}_h \in \mathbb{R}^h$. We represent the partial derivatives of a vectorial function $\mathbf{a} = \mathbf{a}(\mathbf{z}) \in \mathbb{R}^g$ and scalar function $a = a(\mathbf{z}) \in \mathbb{R}$ with respect to $\mathbf{z} \in \mathbb{R}^h$ by[3]

$$\partial_{\mathbf{z}}\mathbf{a} = \frac{\partial \mathbf{a}}{\partial \mathbf{z}} \in \mathbb{R}^{g\times h}, \qquad \partial_{\mathbf{z}} a = \frac{\partial a}{\partial \mathbf{z}} \in \mathbb{R}^{1\times h}. \tag{1}$$

We represent the Hessian matrix by $\partial_{\mathbf{zz}} a \in \mathbb{R}^{h\times h}$ and the weighted-Euclidean norm by $\|\mathbf{a}\|_{\mathbf{Z}} = \mathbf{a}^\top \mathbf{Z}\mathbf{a}$, for a symmetric matrix $\mathbf{Z} = \mathbf{Z}^\top$ of appropriate dimensions.

B. Hamiltonian Dynamics

Consider a nonredundant serial robot manipulator, with n rotational degrees of freedom (DOF). We denote the vectors of joint and end-effector displacements by $\mathbf{q} \in \mathbb{R}^n$ and $\mathbf{x} = \mathbf{x}(\mathbf{q}) \in \mathbb{R}^n$, respectively. The manipulator's end-effector physically interacts with a lossless environment, which imposes m elastically constrained directions (where $n \geq m$). Similar to [24], we locally decompose the coordinates of $\mathbf{x}$ as

$$\mathbf{x} = [\mathbf{r}^\top \quad \mathbf{s}^\top]^\top \tag{2}$$

where $\mathbf{r} \in \mathbb{R}^m$ and $\mathbf{s} \in \mathbb{R}^{n-m}$ represent the vectors of constrained and unconstrained displacements, respectively. Physically, $m = n$ represents a manipulator that can apply force to the environment in any direction, while $m = 1$ represents, e.g., point interaction with one deformable surface. The energy storage function (i.e., the Hamiltonian) of this elastically constrained mechanism is given by

$$\mathcal{H}(\mathbf{q}, \mathbf{p}) = \frac{1}{2}\mathbf{p}^\top \mathbf{M}^{-1}(\mathbf{q})\mathbf{p} + \mathcal{V}(\Delta\mathbf{r}) \in \mathbb{R} \tag{3}$$

where $\mathbf{M}(\mathbf{q}) \in \mathbb{R}^{n\times n}$ denotes the standard mass matrix and $\mathbf{p} \in \mathbb{R}^n$ represents the system's momenta, which satisfies $\mathbf{p} = \mathbf{M}(\mathbf{q})\dot{\mathbf{q}}$. For ease of presentation, we assume that no gravitational potential is present on the system. This way, the potential function $\mathcal{V}(\Delta\mathbf{r}) \in \mathbb{R}$ only models the elastic energy induced by the environment. The vector $\Delta\mathbf{r} = \mathbf{r} - \mathbf{r}_{\text{eq}} \in \mathbb{R}^n$ represents the relative constrained displacement, for $\mathbf{r}_{\text{eq}}$ as the constant undeformed equilibrium.

We model the dynamic equations of this system by [6]

$$\begin{bmatrix} \dot{\mathbf{q}} \\ \dot{\mathbf{p}} \end{bmatrix} = \begin{bmatrix} \mathbf{0}_{n\times n} & \mathbf{I}_{n\times n} \\ -\mathbf{I}_{n\times n} & -\mathbf{B} \end{bmatrix} \begin{bmatrix} \partial_{\mathbf{q}}\mathcal{H}^\top \\ \partial_{\mathbf{p}}\mathcal{H}^\top \end{bmatrix} + \begin{bmatrix} \mathbf{0}_n \\ \mathbf{u} \end{bmatrix} \tag{4}$$

where $\mathbf{u} \in \mathbb{R}^n$ denotes the control input and $\mathbf{B} > 0 \in \mathbb{R}^{n\times n}$ represents a symmetric dissipation matrix.

Assumption 1 [16], [17]: The elastic energy $\mathcal{V}(\Delta\mathbf{r})$ induced by the lossless environment is a smooth positive-definite potential function, with a unique constant equilibrium, whose gradient $\partial_{\mathbf{r}}\mathcal{V}(\Delta\mathbf{r})$ is strictly increasing with respect to $\Delta\mathbf{r}$, and its Hessian matrix satisfies $\partial_{\mathbf{rr}}\mathcal{V}(\Delta\mathbf{r}) \geq 0$.

C. Canonical Change of Coordinates

Instrumental for our control design is to perform the coordinate transformation $(\mathbf{q}, \mathbf{p}) \mapsto (\mathbf{x}, \boldsymbol{\pi})$. To this end, we define the new momenta variable

$$\boldsymbol{\pi} = \mathbf{T}(\mathbf{x})\mathbf{J}^{-\top}(\mathbf{q})\mathbf{p} \in \mathbb{R}^n \tag{5}$$

where $\mathbf{T}(\mathbf{x}) = \mathbf{T}^\top(\mathbf{x}) > 0 \in \mathbb{R}^{n\times n}$ represents a positive-definite symmetric matrix (whose explicit definition is given in later sections) and $\mathbf{J}(\mathbf{q}) = \partial_{\mathbf{q}}\mathbf{x}(\mathbf{q}) \in \mathbb{R}^{n\times n}$ denotes the Jacobian matrix of the manipulator. We assume that the configuration of the system is such that $\mathbf{J}(\mathbf{q})$ is always full rank. Thus, this coordinate transformation is valid only locally.

The dynamical system (4) expressed in terms of the new coordinates $(\mathbf{x}, \boldsymbol{\pi})$ is given by (see [25] for details)

$$\begin{bmatrix} \dot{\mathbf{x}} \\ \dot{\boldsymbol{\pi}} \end{bmatrix} = \begin{bmatrix} \mathbf{0}_{n\times n} & \mathbf{T}(\mathbf{x}) \\ -\mathbf{T}(\mathbf{x}) & -\mathbf{C}(\mathbf{x}, \boldsymbol{\pi}) \end{bmatrix} \begin{bmatrix} \partial_{\mathbf{x}}\bar{\mathcal{H}}^\top \\ \partial_{\boldsymbol{\pi}}\bar{\mathcal{H}}^\top \end{bmatrix} + \begin{bmatrix} \mathbf{0}_n \\ \mathbf{T}(\mathbf{x})\mathbf{v} \end{bmatrix} \tag{6}$$

with a matrix $\mathbf{C}(\mathbf{x}, \boldsymbol{\pi}) = \mathbf{C}_{\text{skew}}(\mathbf{x}, \boldsymbol{\pi}) + \mathbf{C}_{\text{sym}}(\mathbf{x}, \boldsymbol{\pi}) \in \mathbb{R}^{n\times n}$ composed of a symmetric and skew-symmetric parts

$$\mathbf{C}_{\text{skew}}(\mathbf{x}, \boldsymbol{\pi}) = \mathbf{T}(\mathbf{x})\mathbf{J}^{-\top}(\mathbf{q})\partial_{\mathbf{q}}\boldsymbol{\pi}^\top - \partial_{\mathbf{q}}\boldsymbol{\pi}\mathbf{J}^{-1}(\mathbf{q})\mathbf{T}(\mathbf{x}) \tag{7}$$

$$\mathbf{C}_{\text{sym}}(\mathbf{x}, \boldsymbol{\pi}) = \mathbf{T}(\mathbf{x})\mathbf{J}^{-\top}(\mathbf{q})\mathbf{B}\mathbf{J}^{-1}(\mathbf{q})\mathbf{T}(\mathbf{x}) \tag{8}$$

[3]Note the abuse of notation using $\mathbf{a}(\mathbf{z})$ as both a coordinate vector and a vectorial function.

and a new control input (which represents end-effector forces)

$$\mathbf{v} = \mathbf{J}^{-\top}(\mathbf{q})\mathbf{u} \in \mathbb{R}^n. \tag{9}$$

The energy function (3) expressed in these coordinates is

$$\bar{\mathcal{H}}(\mathbf{x}, \boldsymbol{\pi}) = \frac{1}{2}\boldsymbol{\pi}^\top \mathbf{M}_x^{-1}(\mathbf{x})\boldsymbol{\pi} + \mathcal{V}(\Delta\mathbf{r}) \tag{10}$$

where we define the $n \times n$ mass-like matrix

$$\mathbf{M}_x(\mathbf{x}) = \mathbf{T}(\mathbf{x})\mathbf{J}^{-\top}(\mathbf{q})\mathbf{M}(\mathbf{q})\mathbf{J}^{-1}(\mathbf{q})\mathbf{T}(\mathbf{x})|_{\mathbf{q}=\mathbf{q}(\mathbf{x})}. \tag{11}$$

We discuss the advantages of performing this canonical coordinate transformation in later sections.

D. Energy-Based Modeling of the Force Measurements

As in [23], we model the interaction forces between the manipulator and the environment by

$$\mathbf{R}(\mathbf{q})\mathbf{f}_\mathrm{S} = \partial_\mathbf{r}\mathcal{V}(\Delta\mathbf{r})^\top \in \mathbb{R}^m \tag{12}$$

where the vector $\mathbf{f}_\mathrm{S} \in \mathbb{R}^m$ represents the measurements of a force transducer (conveniently located at the contact point) and $\mathbf{R}(\mathbf{q}) \in \mathbb{R}^{m\times m}$ represents a known transformation matrix from world (base) coordinates to end-effector (sensor) coordinates. To simplify notation, we define the following vector of interaction forces in world coordinates:

$$\mathbf{f} = \mathbf{R}(\mathbf{q})\mathbf{f}_\mathrm{S} \in \mathbb{R}^m. \tag{13}$$

III. Standard Energy Shaping

In this section, we present and analyze the properties of a force regulator derived using standard energy shaping methods, i.e., only shaping the potential energy function.

A. Ideal Scenario

The aim of the standard energy shaping control is to design a static-state feedback regulator, which enforces a desired potential energy function $\mathcal{V}_d(\Delta\tilde{\mathbf{r}}) \in \mathbb{R}$ into the closed-loop system (see [26]–[28] for details). To achieve force regulation, this potential function must have a minimum at the desired configuration. This means that the equilibrium point

$$\Delta\tilde{\mathbf{r}} = \Delta\mathbf{r} - \Delta\mathbf{r}^* = \mathbf{0}_m \in \mathbb{R}^m \tag{14}$$

with $\Delta\mathbf{r}^* = \mathbf{r}^* - \mathbf{r}_\mathrm{eq} \in \mathbb{R}^m$ as an unknown constant displacement must imply the application of the constant reference force $\mathbf{f}^* \in \mathbb{R}^m$. Following the energy-based model (12) and (13), this reference force satisfies the relation:

$$\mathbf{f}^* = \partial_\mathbf{r}\mathcal{V}(\Delta\mathbf{r}^*)^\top. \tag{15}$$

Note that since the analytical expression of $\mathcal{V}(\Delta\mathbf{r})$ is not known, then, we cannot *a priori* compute a constant displacement $\Delta\mathbf{r}^*$ at which the force $\mathbf{f}^*$ is exactly applied.

Proposition 1: Consider the system (6) in closed loop with

$$\mathbf{v} = -\begin{bmatrix} k_f\tilde{\mathbf{f}} - \mathbf{f}^* \\ k_s\tilde{\mathbf{s}} \end{bmatrix} + \boldsymbol{\upsilon} \tag{16}$$

with errors $\tilde{\mathbf{f}} = \mathbf{f} - \mathbf{f}^* \in \mathbb{R}^m$ and $\tilde{\mathbf{s}} = \mathbf{s} - \mathbf{s}^* \in \mathbb{R}^{n-m}$, constant reference $\mathbf{s}^* \in \mathbb{R}^{n-m}$, positive feedback gains $k_f, k_s \in \mathbb{R}$, and external control input $\boldsymbol{\upsilon} \in \mathbb{R}^n$. The control law (16) enforces the storage function

$$\mathcal{L}(\mathbf{x}, \boldsymbol{\pi}) = \frac{1}{2}\boldsymbol{\pi}^\top \mathbf{M}_x^{-1}(\mathbf{x})\boldsymbol{\pi} + \mathcal{V}_d(\Delta\tilde{\mathbf{r}}) + \frac{1}{2}k_s\tilde{\mathbf{s}} \cdot \tilde{\mathbf{s}} \tag{17}$$

where the elastic energy $\mathcal{V}_d(\Delta\tilde{\mathbf{r}}) \in \mathbb{R}$ has a unique minimum at which the constant force $\mathbf{f}^*$ is exerted onto the environment.

Proof: We can alternatively express the controller (16) as

$$\mathbf{v} = -\partial_\mathbf{x}\left\{\mathcal{V}_a(\Delta\mathbf{r}) + \frac{1}{2}k_s\tilde{\mathbf{s}} \cdot \tilde{\mathbf{s}}\right\} + \boldsymbol{\upsilon} \tag{18}$$

for an added elastic energy function

$$\mathcal{V}_a(\Delta\mathbf{r}) = k_f\mathcal{V}(\Delta\mathbf{r}) - K\mathbf{r} \cdot \partial_\mathbf{r}\mathcal{V}(\Delta\mathbf{r}^*) + \varepsilon \in \mathbb{R} \tag{19}$$

with $K = k_f + 1 \in \mathbb{R}$ and arbitrary integration scalar $\varepsilon \in \mathbb{R}$. Direct substitution of (18) into (6) enforces (17) (the standard potential shaping) with shaped elastic energy

$$\begin{aligned} \mathcal{V}_d(\Delta\tilde{\mathbf{r}}) &= \mathcal{V}(\Delta\mathbf{r}) + \mathcal{V}_a(\Delta\mathbf{r}) \\ &\geq 0 \\ &= K(\mathcal{V}(\Delta\mathbf{r}) - \mathcal{V}(\Delta\mathbf{r}^*) - \tilde{\mathbf{r}} \cdot \partial_\mathbf{r}\mathcal{V}(\Delta\mathbf{r}^*)) \end{aligned} \tag{20}$$

where we set $\varepsilon = K(\mathbf{r}^* \cdot \partial_\mathbf{r}\mathcal{V}(\Delta\mathbf{r}^*) - \mathcal{V}(\Delta\mathbf{r}^*))$. We prove the desired equilibrium by noting that the first-order Taylor's expansion of $\mathcal{V}(\Delta\mathbf{r})$ around $\mathbf{r}^*$ satisfies

$$\mathcal{V}(\Delta\mathbf{r}) > \mathcal{V}(\Delta\mathbf{r}^*) + \tilde{\mathbf{r}} \cdot \partial_\mathbf{r}\mathcal{V}(\Delta\mathbf{r}^*) \quad \forall\mathbf{r} \neq \mathbf{r}^* \tag{21}$$

which means that $\Delta\mathbf{r}^*$ is a minimum for $\mathcal{V}_d(\Delta\tilde{\mathbf{r}})$. ■

B. Uncalibrated Scenario

Despite the nice properties of the previous control design, it is well known that, in real applications, it is difficult to achieve asymptotic force regulation with simple proportional and feedforward control actions [29]. Note that to ensure that $\tilde{\mathbf{f}} = \mathbf{0}_m$ is an equilibrium for $\mathcal{V}_d(\Delta\tilde{\mathbf{r}})$, the constant feedforward term $\mathbf{f}^*$ must exactly compensate the environment's elastic force at the desired configuration $\Delta\mathbf{r}^*$. If this static compensation is not satisfied, the interaction force presents the typical steady-state deviation, call it $\mathbf{d} \in \mathbb{R}^m$, from its reference. In our approach, we model this situation by introducing $\mathbf{d}$ as a constant disturbance to the closed-loop system that arises from substituting (18) into (6)

$$\begin{bmatrix} \dot{\mathbf{x}} \\ \dot{\boldsymbol{\pi}} \end{bmatrix} = \begin{bmatrix} \mathbf{0}_{n\times n} & \mathbf{T}(\mathbf{x}) \\ -\mathbf{T}(\mathbf{x}) & -\mathbf{C}(\mathbf{x}, \boldsymbol{\pi}) \end{bmatrix}\begin{bmatrix} \partial_\mathbf{x}\mathcal{L}^\top \\ \partial_{\boldsymbol{\pi}}\mathcal{L}^\top \end{bmatrix} + \begin{bmatrix} \mathbf{0}_n \\ \mathbf{T}(\mathbf{x})(\mathbf{d}_x + \boldsymbol{\upsilon}) \end{bmatrix} \tag{22}$$

for $\mathbf{d}_x = [\mathbf{d}^\top, \mathbf{0}_{n-m}^\top]^\top \in \mathbb{R}^n$. We use the disturbance $\mathbf{d}$ to model the common uncalibrated scenario where the numerical control law does not exactly match the real physical input (i.e., the joint forces/torques). From this expression, we see that, at steady state, the following relation arises:

$$-\partial_\mathbf{r}\mathcal{V}_d(\Delta\tilde{\mathbf{r}})^\top + \mathbf{d} \equiv \mathbf{0}_m \tag{23}$$

which shows that, as expected, the controller can no longer guarantee asymptotic stability. We use this simple example to motivate our control developments in the following section.

IV. Robust Energy Shaping

In this section, we present an energy shaping approach that allows to incorporate integral force controls within the port-Hamiltonian framework.

A. Displacement-Independent Kinetic Energy

Following the approach reported in [30], we define $\mathbf{T}(\mathbf{x})$ as the square root matrix of $\mathbf{J}(\mathbf{q})\mathbf{M}^{-1}(\mathbf{q})\mathbf{J}^{\top}(\mathbf{q})$, that is, as the symmetric and positive-definite matrix[4] that satisfies:

$$\mathbf{T}(\mathbf{x})\mathbf{T}(\mathbf{x}) = \mathbf{J}(\mathbf{q})\mathbf{M}^{-1}(\mathbf{q})\mathbf{J}^{\top}(\mathbf{q})|_{\mathbf{q}=\mathbf{q}(\mathbf{x})}. \tag{24}$$

The motivation behind the coordinate transformation $(\mathbf{q}, \mathbf{p}) \mapsto (\mathbf{x}, \boldsymbol{\pi})$ is to render the kinetic energy in terms of the end-effector motion and independent of the displacements vector. Note that with this definition of $\mathbf{T}(\mathbf{x})$, the closed-loop energy storage (17) now satisfies

$$\mathcal{L}(\mathbf{x}, \boldsymbol{\pi}) = \frac{1}{2}\boldsymbol{\pi} \cdot \boldsymbol{\pi} + \mathcal{U}(\tilde{\mathbf{x}}) \tag{25}$$

where to simplify notation, we define the potential function

$$\mathcal{U}(\tilde{\mathbf{x}}) = \mathcal{V}_d(\Delta\tilde{\mathbf{r}}) + \frac{1}{2}k_s\tilde{\mathbf{s}} \cdot \tilde{\mathbf{s}} \in \mathbb{R} \tag{26}$$

for an error vector $\tilde{\mathbf{x}} = \mathbf{x} - \mathbf{x}^* \in \mathbb{R}^n$, with a constant reference $\mathbf{x}^* = [\Delta\mathbf{r}^{*\top}, \mathbf{s}^{*\top}]^{\top} \in \mathbb{R}^n$.

Remark 1: To compute the square-root matrix $\mathbf{T}(\mathbf{x})$, we do not need to know its exact analytical expression (which for more than 2-DOF is difficult to obtain). For that, in Appendix A, we present an algorithm that computes this matrix from the mass and Jacobian matrices.

B. Momenta Controller

To incorporate integral controls within our formulation, we define the virtual momenta variable [21]

$$\mathbf{z} = \boldsymbol{\pi} + k_\pi \partial_{\mathbf{x}}\mathcal{U}(\tilde{\mathbf{x}})^{\top} \in \mathbb{R}^n \tag{27}$$

with $k_\pi > 0 \in \mathbb{R}$ as a feedback gain. In contrast with the free-motion case in [21], note that we explicitly construct the first m coordinates of (27) with force feedback errors.

Proposition 2: Consider the closed-loop system (22), with a matrix $\mathbf{T}(\mathbf{x})$ satisfying (24). For this situation, there exists a state-feedback control input $\boldsymbol{\upsilon}$, which enforces

$$\begin{bmatrix}\dot{\mathbf{x}}\\ \dot{\mathbf{z}}\end{bmatrix} = \begin{bmatrix}-k_\pi\mathbf{T}(\mathbf{x}) & \mathbf{T}(\mathbf{x})\\ -\mathbf{T}(\mathbf{x}) & -\mathbf{C}(\mathbf{x}, \mathbf{z})\end{bmatrix}\begin{bmatrix}\partial_{\mathbf{x}}\mathcal{W}^{\top}\\ \partial_{\boldsymbol{\pi}}\mathcal{W}^{\top}\end{bmatrix} + \begin{bmatrix}\mathbf{0}_n\\ \mathbf{T}(\mathbf{x})(\mathbf{d}_x + \boldsymbol{\mu})\end{bmatrix} \tag{28}$$

with an energy storage function

$$\mathcal{W}(\tilde{\mathbf{x}}, \mathbf{z}) = \frac{1}{2}\mathbf{z}\cdot\mathbf{z} + \mathcal{U}(\tilde{\mathbf{x}}) \in \mathbb{R} \tag{29}$$

and a robust control input $\boldsymbol{\mu} \in \mathbb{R}^n$ that will be used later.

Proof: By equating $\dot{\mathbf{x}}$ from (22) with that from (28), we see that the velocity relation is satisfied. By equating the time derivative of (27) with $\dot{\mathbf{z}}$ from (28), we obtain

$$\frac{\mathrm{d}}{\mathrm{d}t}\left\{\boldsymbol{\pi} + k_\pi\partial_{\mathbf{x}}\mathcal{U}(\tilde{\mathbf{x}})^{\top}\right\} = \mathbf{T}(\mathbf{x})\left(\mathbf{d}_x + \boldsymbol{\mu}\right) - \mathbf{T}(\mathbf{x})\partial_{\mathbf{x}}\mathcal{W}^{\top} - \mathbf{C}(\mathbf{x}, \mathbf{z})\partial_{\boldsymbol{\pi}}\mathcal{W}^{\top}. \tag{30}$$

[4]Note that by definition, the square root of a positive-definite symmetric matrix is also a positive-definite symmetric matrix.

We obtain the controller by substituting $\dot{\boldsymbol{\pi}}$ from (22) and solving for $\boldsymbol{\upsilon}$

$$\boldsymbol{\upsilon} = -\mathbf{T}^{-1}(\mathbf{x})(\mathbf{C}(\mathbf{x}, \boldsymbol{\pi})k_\pi\partial_{\mathbf{x}}\mathcal{U}(\tilde{\mathbf{x}})^{\top} + k_\pi\partial_{\mathbf{xx}}\mathcal{U}(\tilde{\mathbf{x}})\dot{\mathbf{x}}) + \boldsymbol{\mu}. \tag{31}$$

■

Remark 2: It is important to distinguish between the canonical coordinate transformation of Section II and the actuated coordinate transformation of (28). The motivation of the latter one is to virtually enforce a momenta-like variable, which contains a component of force-position errors (a similar procedure as with the nominal error dynamics in passivity-based controllers for Euler–Lagrange systems [31]). The main difference with our Hamiltonian approach is the introduction of the virtual dissipation element $k_\pi\mathbf{T}(\mathbf{x})$ that appears at the (1, 1) subblock of the interconnection–dissipation matrix in (28). This effort-controlled dissipator (which contrast with the more common flow-controlled dissipator [32]) is crucial to preserve skew symmetry when an integral action is introduced. Note that we can use this simple dissipation analogy to design the feedback gain k_π, i.e., large values of k_π may result in a faster minimization of the error.

Remark 3: To implement the controller (31), we must compute the skew-symmetric matrix in (7) and the Hessian matrix of the elastic energy. We can considerably reduce the apparent complexity in the computation of $\mathbf{C}_{\text{skew}}(\mathbf{x}, \boldsymbol{\pi})$—specifically the partial derivatives of $\mathbf{T}(\mathbf{x})$—using the simplification that we provide in Appendix B. As for the latter control term, note that the analytical expression of $\mathcal{V}(\Delta\mathbf{r})$ is unknown. To solve this issue, in Appendix C, we provide simple algorithms to numerically compute this term in RT.

C. Robustification via Integral Control Design

To enforce asymptotic stability of force errors, we incorporate an extra m-dimensional numerical state into the closed-loop dynamics. This integrator is introduced through the first m coordinates of the robust control port $\boldsymbol{\mu}$, that is

$$\boldsymbol{\mu} = \begin{bmatrix}\boldsymbol{\mu}_1^{\top} & \mathbf{0}_{n-m}^{\top}\end{bmatrix}^{\top} \tag{32}$$

where $\boldsymbol{\mu}_1 \in \mathbb{R}^m$ represents the actuated coordinates.

Assumption 2: For our controller design, we assume that the algorithm in Appendix C exactly computes the first m coordinates of the second control term in (31), i.e., $\partial_{\mathbf{rr}}\mathcal{V}_d(\Delta\tilde{\mathbf{r}})\dot{\mathbf{r}}$.

Proposition 3: The closed-loop system that arises from substituting (31) into (22), with robust control input

$$\boldsymbol{\mu}_1 = -\boldsymbol{\sigma} \tag{33}$$

for a numerical state defined as

$$\dot{\boldsymbol{\sigma}} = k_\sigma\mathbf{T}_{n\times m}^{\top}(\mathbf{x})\mathbf{z} \in \mathbb{R}^m \tag{34}$$

with a positive gain $k_\sigma \in \mathbb{R}$, and a matrix $\mathbf{T}_{n\times m}(\mathbf{x}) \in \mathbb{R}^{n\times m}$ as the $n \times m$ left submatrix of $\mathbf{T}(\mathbf{x}) = [\mathbf{T}_{n\times m}(\mathbf{x}), *]$ is endowed with asymptotic stability of force errors.

Proof: Substitution of (31) into (22) yields the extended port-Hamiltonian system

$$\dot{\boldsymbol{\chi}} = \mathbf{Q}(\boldsymbol{\chi})\partial_{\boldsymbol{\chi}}\mathcal{J}(\boldsymbol{\chi})^{\top} \tag{35}$$

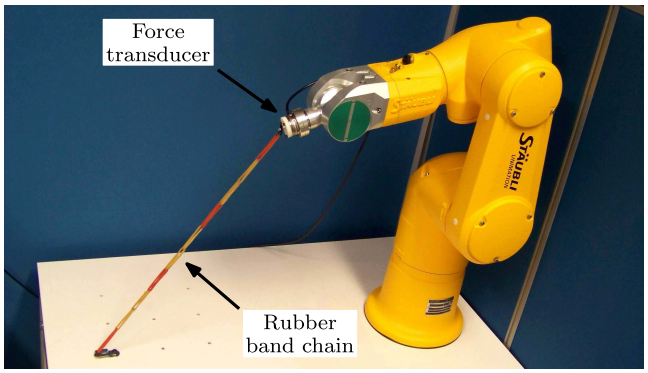

Fig. 1. Robot manipulator used in our experimental study. We instrument this system with an ATI Mini40 force transducer.

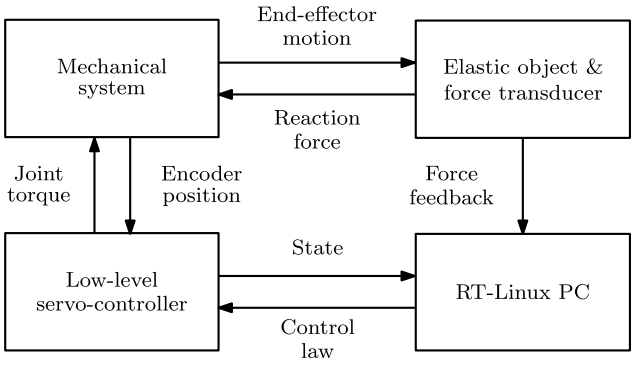

Fig. 2. Conceptual representation of the RT control architecture of the torque-controlled mechanical system.

for an N-dimensional (where $N = 2n+m$) vector of extended state variables

$$\boldsymbol{\chi} = [\mathbf{x}^\top \quad \mathbf{z}^\top \quad \boldsymbol{\sigma}^\top]^\top \in \mathbb{R}^N \tag{36}$$

an $N \times N$ interconnection–dissipation matrix [28]

$$\mathbf{Q}(\mathbf{x}, \mathbf{z}) = \begin{bmatrix} -k_\pi \mathbf{T}(\mathbf{x}) & \mathbf{T}(\mathbf{x}) & \mathbf{0}_{n\times m} \\ -\mathbf{T}(\mathbf{x}) & -\mathbf{C}(\mathbf{x}, \mathbf{z}) & -k_\sigma \mathbf{T}_{n\times m}(\mathbf{x}) \\ \mathbf{0}_{m\times n} & k_\sigma \mathbf{T}^\top_{n\times m}(\mathbf{x}) & \mathbf{0}_{m\times m} \end{bmatrix} \tag{37}$$

and a closed-loop energy function

$$\mathcal{J}(\boldsymbol{\chi}) = \mathcal{W}(\tilde{\mathbf{x}}, \mathbf{z}) + \frac{1}{2k_\sigma}(\boldsymbol{\sigma} - \mathbf{d}) \cdot (\boldsymbol{\sigma} - \mathbf{d}) \in \mathbb{R}. \tag{38}$$

Note that $\mathcal{J}(\boldsymbol{\chi})$ qualifies as a Lyapunov function since

$$\begin{aligned} \dot{\mathcal{J}}(\boldsymbol{\chi}) &= -k_\pi \|\partial_{\mathbf{x}} \mathcal{J}(\boldsymbol{\chi})\|^2_{\mathbf{T}} - \|\partial_{\mathbf{z}} \mathcal{J}(\boldsymbol{\chi})\|^2_{\mathbf{C}_{\text{sym}}} \\ &\leq 0 \quad \forall \boldsymbol{\chi}. \end{aligned} \tag{39}$$

This proves that $(\mathbf{x}^*, \mathbf{0}_n, \mathbf{d})$ is a stable equilibrium of the system. Asymptotic stability of force (and position) errors directly follows by invoking the LaSalle principle [33]. ■

Remark 4: We recently developed in [34] a new energy shaping method to further robustify a force control law similar to (31). Since the method in [34] enforces input-to-state stability [35], thus, it helps to passively reject bounded disturbances (modeling, e.g., uncertain estimations or measurement noise) from the closed-loop system.

V. Experimental Validation

A. Setup

We test the performance of our force control method with a TX-60 Staubli robot manipulator (Fig. 1). In this experimental study, we attach an elastic chain made with rubber bands to the manipulator's end-effector. To measure the interaction forces with the elastic environment, we instrument the manipulator with an ATI Mini40 force transducer.

The Staubli robot has with a low-level interface [36] that allows us to set the torque control input of each joint. To provide a deterministic RT behavior to the control algorithms (a key feature to guarantee a constant and small sample time), we use a Xenomai-patched RT-Linux PC [37] to process the feedback signals and compute the control law; we send this torque command via TCP/IP to the low-level servo controller.

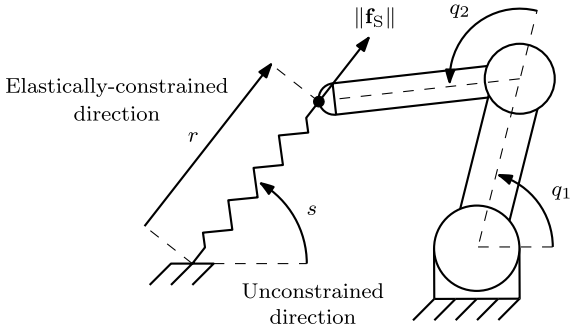

Fig. 3. Conceptual representation of the elastically constrained and unconstrained directions of the mechanical system.

We implement all the algorithms at an RT servo loop of $\delta t = 4$ ms. Fig. 2 shows a conceptual representation of the control architecture.

We conduct this experimental study with the setup conceptually shown in Fig. 3. Note that we use the elastic chain to perform dynamically rich movements[5] without losing physical interaction. In this brief, we only consider motion of the manipulator's second and third joints. This provides a planar elbow configuration with $\mathbf{q} = [q_1, q_2]^\top \in \mathbb{R}^2$. We represent the end-effector position $\mathbf{x} = [r, s]^\top \in \mathbb{R}^2$ with polar coordinates, where $r \in \mathbb{R}$ denotes the linear constrained displacement and $s \in \mathbb{R}$ is the angular unconstrained displacement. We compute the interaction force by $f = \|\mathbf{f}_S\| \in \mathbb{R}$. To implement the controller, we use $k_f = 25$, $k_s = 500$, $k_\pi = 0.05$, and $k_\sigma = 25$. The design of the gains k_f and k_s follows that of standard proportional feedback, k_π represents an error dissipator (thus small values make convergence slower/smoother), and k_σ modulates the integral action.

B. Experiments With Standard and Robust Energy Shaping

To test the stability of our controller, we apply impulse-like external perturbations to the closed-loop mechanical system. We do this by manually pulling the stretched elastic chain from the desired equilibrium (i.e., from zero initial force and position errors). We set the desired force and position references to $f^* = 10$ N and $s^* = 65°$.

[5]For slow motions, all the inertia-dependent terms are negligible, i.e., friction and potential forces become the dominating effects in the system.

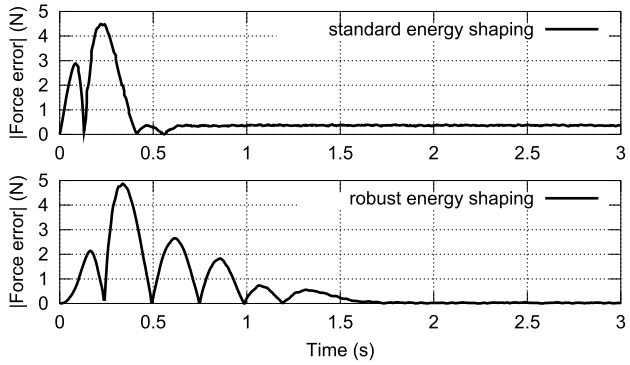

Fig. 4. Comparison of the force error $|\tilde{f}|$ obtained with the standard potential energy shaping approach and the robust force controller.

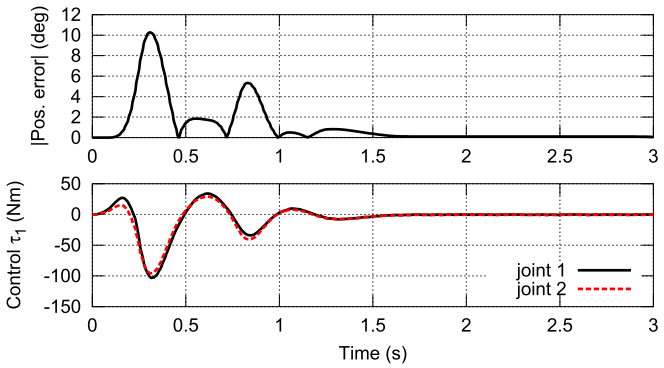

Fig. 5. Time evolution of the unconstrained position error $|\tilde{s}|$ (obtained with the robust controller) and the potential shaping control action $\boldsymbol{\tau}_1$.

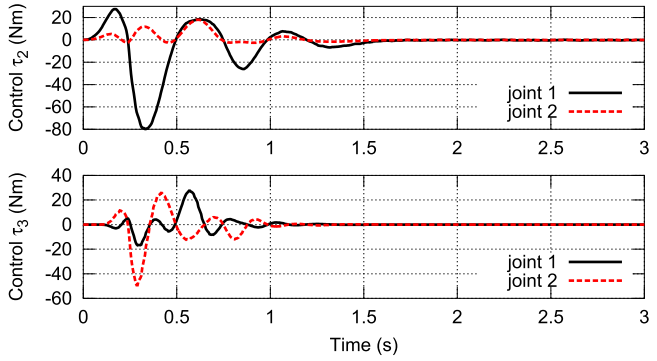

Fig. 6. Time evolution of the $\boldsymbol{\tau}_2$ and $\boldsymbol{\tau}_3$ joint control actions of the proposed momenta controller.

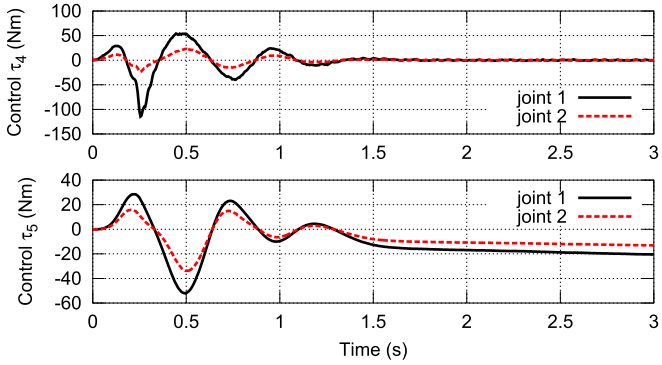

Fig. 7. Time evolution of the $\boldsymbol{\tau}_4$ control actions of the momenta controller and the robust control action $\boldsymbol{\tau}_5$ of the proposed asymptotic force regulator.

Fig. 4 shows a comparison of the force error $|\tilde{f}|$ obtained with the controller (16) with $\boldsymbol{\upsilon} = \mathbf{0}_n$ [Fig. 4 (top)], and with $\boldsymbol{\upsilon}$ as in (31) and $\boldsymbol{\mu}_1$ as in (33) [Fig. 4 (bottom)]. The first case corresponds to the standard energy shaping design, while the second case corresponds to the robust controller. This figure shows that with the static-state feedback control approach, a constant bias is not compensated. As expected, we obtain asymptotic stability by incorporating the port-Hamiltonian integral action. The top part of Fig. 5 shows the unconstrained position error $|\tilde{s}|$ that is obtained with the robust energy shaping design.

To analyze the specific contribution of each control action in (31), consider the following decomposition of the joint torque input that arises by solving (9) for $\mathbf{u}$:

$$\begin{aligned}\mathbf{u} = &\underbrace{-\mathbf{J}^{\top}(\mathbf{q})\partial_{\mathbf{x}}\mathcal{U}(\tilde{\mathbf{x}})^{\top}}_{-\boldsymbol{\tau}_1} \underbrace{-\mathbf{B}\mathbf{J}_{\mathrm{T}}^{-1}(\mathbf{q})k_{\pi}\partial_{\mathbf{x}}\mathcal{U}(\tilde{\mathbf{x}})^{\top}}_{-\boldsymbol{\tau}_2} \\ &\underbrace{+\mathbf{J}_{\mathrm{T}}^{\top}(\mathbf{q})\mathbf{C}_{\mathrm{skew}}(\mathbf{q},\boldsymbol{\pi})k_{\pi}\partial_{\mathbf{x}}\mathcal{U}(\tilde{\mathbf{x}})^{\top}}_{\boldsymbol{\tau}_3} \\ &\underbrace{-\mathbf{J}_{\mathrm{T}}^{\top}(\mathbf{q})k_{\pi}\partial_{\mathbf{x}\mathbf{x}}\mathcal{U}(\tilde{\mathbf{x}})\dot{\mathbf{x}}}_{-\boldsymbol{\tau}_4} \underbrace{-\mathbf{J}^{\top}(\mathbf{q})\begin{bmatrix}\sigma\\0\end{bmatrix}}_{-\boldsymbol{\tau}_5} \in \mathbb{R}^2 \end{aligned} \tag{40}$$

for $\mathbf{J}_{\mathrm{T}}^{\top}(\mathbf{q}) = \mathbf{J}^{\top}(\mathbf{q})\mathbf{T}^{-1}(\mathbf{q}) \in \mathbb{R}^{2\times 2}$.

The bottom part of Fig. 5 shows the time evolution of the standard potential shaping control $\boldsymbol{\tau}_1$. The terms $\boldsymbol{\tau}_2$, $\boldsymbol{\tau}_3$, and $\boldsymbol{\tau}_4$ represent the different actions of the proposed momenta controller. The top and bottom parts of Fig. 6 show the time evolution of the damping-like $\boldsymbol{\tau}_2$ and skew-symmetric $\boldsymbol{\tau}_3$ control actions, respectively. The top and bottom parts of Fig. 7 show the computed term $\boldsymbol{\tau}_4$ and the joint torque corresponding to the force integral action $\boldsymbol{\tau}_5$, respectively. Note that with respect to the previous momenta controls, $\boldsymbol{\tau}_4$ shows an increased magnitude and the presence of noise. For simplicity, we compute $\boldsymbol{\tau}_4$ using a filtered version of the first method described in Appendix C. These results experimentally prove the proposed theory, i.e., that the force error is minimized by compensating the unknown bias with the integrator's action.

C. Comparison of the Computation Methods for $\partial_{\mathbf{rr}}\mathcal{U}(\Delta\tilde{\mathbf{r}})\dot{\mathbf{r}}$

The aim of this experimental study is simply to compare the online numerical methods detailed in Appendix C, therefore no force control is performed. We conduct this brief with the same setup shown in Fig. 1. To qualitatively compare the methods, we move the end effector along an arbitrary trajectory, while simultaneously estimate the term $\partial_{\mathbf{rr}}\mathcal{U}(\Delta\tilde{\mathbf{r}})\dot{\mathbf{r}}$. Fig. 8 shows the trajectory of the constrained displacement r and the measured interaction force f.

Fig. 9 shows a graphical comparison of the measured force difference (i.e., the unfiltered secant method)

$$\delta f(t) = f(t) - f(t-\delta t) \in \mathbb{R} \tag{41}$$

and the force differences $\widehat{\delta f}(t)$ computed with the Broyden and gradient-descent rules (as detailed in Appendix C),

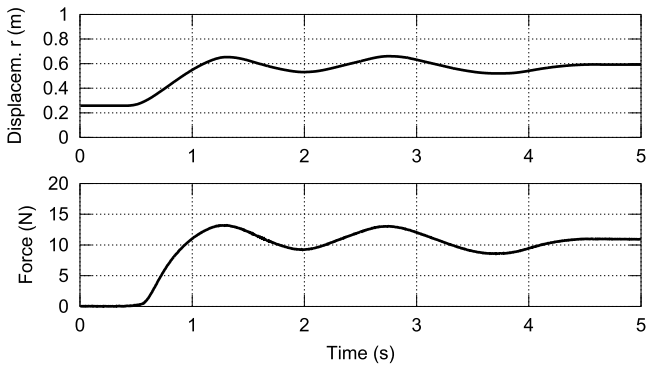

Fig. 8. Constrained displacement r and force f profiles that we use for the experimental comparison of the online methods described in Appendix C.

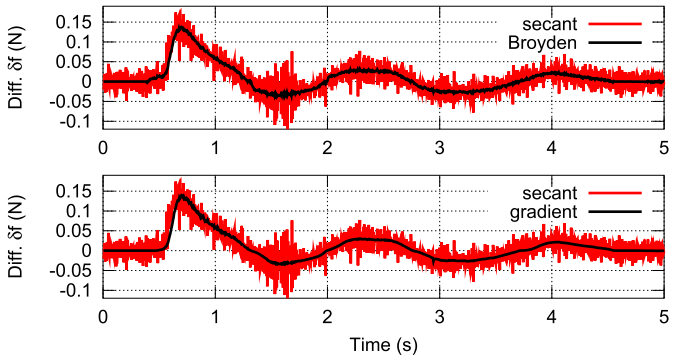

Fig. 9. Comparison of the measured force difference $\delta f(t)$ and the ones computed with the Broyden (above) and gradient-descent (below) update rules.

with $K = 1$. From these results, we see that $\partial_{\mathbf{rr}}\mathcal{U}(\Delta\tilde{\mathbf{r}})\dot{\mathbf{r}}$ is closely approximated by both methods. Note that these methods compute the unknown term mostly from state variables (where we use a minimum of force information just to update the model) and present a little noise, therefore they are suitable for model-based control. We obtain these results using the Broyden method with a gain $\Gamma = 0.2$ (small values help to filter out noise) and using the gradient-descent method with approximated nonlinear model $f \approx \eta_1 r + \eta_2 r^2 + \eta_3 r^3$ and gain $k_\eta = 5 \times 10^6$.

VI. Conclusion

In this brief, we presented an energy shaping method to control the interaction forces between a mechanical system and a compliant environment. Our asymptotic controller was designed in a constructive manner: we first derived a standard potential shaping control action, then we incorporated a state-feedback momenta control component, and finally we robustified the method by including integral force controls. We presented the experimental results to validate our method.

The canonical coordinate transformation (5) results instrumental to preserve in closed-loop the port-Hamiltonian structure. Note that the implementation of our method does not require the explicit analytical forms of the square-root matrix and the environment's stiffness model. For that, we provide numerical algorithms to compute these terms.

As future research is the inclusion of the inertia-dependent terms within an adaptive estimation algorithm. This way, the exact mass parameters of the mechanical system does not need to be exactly identified beforehand.

Appendix A
Computation of $\mathbf{T}$

Consider the symmetric and positive-definite operational space mass matrix $\mathbf{N} = \mathbf{J}^{-\top}\mathbf{M}\mathbf{J}^{-1} \in \mathbb{R}^{n\times n}$. Note that since, locally, $\text{rank}\{\mathbf{N}^{-1}\} = n$, then $\mathbf{N}^{-1}$ is diagonalisable, that is, $\mathbf{N}^{-1} = \mathbf{V}\mathbf{D}\mathbf{V}^{-1}$, where $\mathbf{V} \in \mathbb{R}^{n\times n}$ is a matrix whose columns are the n eigenvectors of $\mathbf{N}^{-1}$, and the diagonal matrix $\mathbf{D} \in \mathbb{R}^{n\times n}$ has as elements the eigenvalues of $\mathbf{N}^{-1}$. We compute the square-root matrix as follows:

$$\mathbf{T} = \mathbf{V}\mathbf{D}^{1/2}\mathbf{V}^{-1}. \tag{42}$$

Free numerical libraries [38] can be employed to compute in RT the eigenvectors and eigenvalues of $\mathbf{N}^{-1}$.

Appendix B
Computation of $\mathbf{C}_{\text{skew}}$

An equivalent expression (with arguments omitted to avoid clutter) of the gyroscopic forces in (6) is as follows:

$$-\mathbf{C}_{\text{skew}}\boldsymbol{\pi} = \partial_{\mathbf{q}}\boldsymbol{\pi}\,\dot{\mathbf{q}} - \mathbf{T}\mathbf{J}^{-\top}\partial_{\mathbf{q}}\left\{\tfrac{1}{2}\mathbf{p}^\top\mathbf{M}^{-1}\mathbf{p}\right\}^\top \tag{43}$$

which comes from time differentiating (5) and grouping the corresponding terms. From [26], we know that the partial derivative $\partial_{\mathbf{q}}\{1/2\mathbf{p}^\top\mathbf{M}^{-1}\mathbf{p}\}^\top = \mathbf{E}\mathbf{p}$, for a matrix

$$\mathbf{E} = \tfrac{1}{2}\partial_{\mathbf{q}}\{\mathbf{p}^\top\mathbf{M}^{-1}\} \in \mathbb{R}^{n\times n}. \tag{44}$$

Since $\mathbf{C}_{\text{skew}} = -\mathbf{C}_{\text{skew}}^\top$, then we compute it by

$$\mathbf{C}_{\text{skew}} = \mathbf{T}\mathbf{J}^{-\top}\mathbf{E}\mathbf{J}^\top\mathbf{T}^{-1} - (\mathbf{T}\mathbf{J}^{-\top}\mathbf{E}\mathbf{J}^\top\mathbf{T}^{-1})^\top \tag{45}$$

which only requires the partial derivatives of the mass matrix.

Appendix C
Computation of $\partial_{\mathbf{rr}}\mathcal{V}_d(\Delta\mathbf{r})\dot{\mathbf{r}}$

A. Secant Method

Note that the sensor-based expression $K\frac{\mathrm{d}}{\mathrm{d}t}\mathbf{f}(t) = \partial_{\mathbf{rr}}\mathcal{V}_d(\Delta\mathbf{r}(t))\dot{\mathbf{r}}(t)$ satisfies for lossless environments. The simplest way to compute this term is to use, for sample time δt, a two-point estimation of the slope

$$k_\pi\,\partial_{\mathbf{rr}}\mathcal{V}_d(\Delta\tilde{\mathbf{r}}(t))\dot{\mathbf{r}}(t) \approx k_\pi K\frac{\mathbf{f}(t) - \mathbf{f}(t-\delta t)}{\delta t}. \tag{46}$$

Since force transducers are usually noisy, a low-pass filter is needed to smooth the right-hand side of the above estimation.

B. Broyden Update Rule

Let $\boldsymbol{\Omega}(t) \in \mathbb{R}^{m\times m}$ denote an estimation of $\partial_{\mathbf{rr}}\mathcal{V}_d(\Delta\tilde{\mathbf{r}}(t))$. Given observations of displacements $\delta\mathbf{r}(t) = \mathbf{r}(t) - \mathbf{r}(t-\delta t)$ and forces $\delta\mathbf{f}(t) = \mathbf{f}(t) - \mathbf{f}(t-\delta t)$, we can iteratively compute $\boldsymbol{\Omega}(t)$ by

$$\boldsymbol{\Omega}(t) = \boldsymbol{\Omega}(t-\delta t) + \Gamma\frac{K\delta\mathbf{f}(t) - \boldsymbol{\Omega}(t-\delta t)\delta\mathbf{r}(t)}{\delta\mathbf{r}(t)^\top\delta\mathbf{r}(t)}\delta\mathbf{r}(t)^\top \quad \forall\delta\mathbf{r}(t) \neq \mathbf{0}_m \tag{47}$$

for $0 < \Gamma \leq 1$ as a tuning gain. For force control applications, small values of Γ help to filter out noise from the sensor

measurements. Note that the update rule does not ensure the estimation of a symmetric matrix, i.e., it only computes a matrix $\mathbf{\Omega}(t)$ that approximates $K\delta\mathbf{f}_i(t) \approx K\widehat{\delta\mathbf{f}}(t) = \mathbf{\Omega}(t)\delta\mathbf{r}(t)$ (see [39] for details).

C. Gradient-Descent Rule

Consider the approximated model $\mathbf{f} \approx \mathbf{A}(\mathbf{r})\boldsymbol{\eta}$, for a regression matrix $\mathbf{A}(\mathbf{r}) \in \mathbb{R}^{m\times\kappa}$ and parameters $\boldsymbol{\eta} \in \mathbb{R}^{\kappa}$. We approximate the discrete difference by $\delta\mathbf{f}(t) \approx \partial_{\mathbf{r}}\{\mathbf{A}(\mathbf{r}(t))\boldsymbol{\eta}\}\delta\mathbf{r}(t) = \mathbf{W}(\mathbf{r}(t), \delta\mathbf{r}(t))\boldsymbol{\eta}$, for a known regression matrix $\mathbf{W}(\cdot) \in \mathbb{R}^{m\times\kappa}$. Given this model, we compute in RT $\widehat{\delta\mathbf{f}}(t) = \mathbf{W}(\mathbf{r}(t), \delta\mathbf{r}(t))\widehat{\boldsymbol{\eta}}(t) \in \mathbb{R}^m$, where we update the variable parameters $\widehat{\boldsymbol{\eta}}(t) \in \mathbb{R}^{\kappa}$ with the gradient-descent rule

$$\widehat{\boldsymbol{\eta}}(t) = \widehat{\boldsymbol{\eta}}(t-\delta t) - \mathbf{W}^{\top}(\mathbf{r}(t), \delta\mathbf{r}(t))k_{\eta}(\widehat{\delta\mathbf{f}}(t) - \delta\mathbf{f}(t)) \quad (48)$$

for a tuning gain $k_{\eta} > 0 \in \mathbb{R}$. With this method, we continuously vary $\widehat{\boldsymbol{\eta}}(t)$ such that the error $[\widehat{\delta\mathbf{f}}(t) - \delta\mathbf{f}(t)]$ is minimized, see [40] for a similar approach.

REFERENCES

[1] G. Fichtinger, P. Kazanzides, A. Okamura, G. Hager, L. Whitcomb, and R. Taylor, "Surgical and interventional robotics: Part II," *IEEE Robot. Autom. Mag.*, vol. 15, no. 3, pp. 94–102, Sep. 2008.

[2] A. Bicchi and G. Tonietti, "Fast and soft-arm tactics [robot arm design]," *IEEE Robot. Autom. Mag.*, vol. 11, no. 2, pp. 22–33, Jun. 2004.

[3] M. Takegaki and S. Arimoto, "A new feedback method for dynamic control of manipulators," *ASME J. Dyn. Syst., Meas., Control*, vol. 102, pp. 119–125, Jun. 1981.

[4] S. Arimoto and F. Miyazaki, "Stability and robustness of PID feedback control for robot manipulators of sensory capability," in *Proc. 1st Int. Symp. Robot. Res.*, 1983, pp. 783–799.

[5] R. Ortega, A. van der Schaft, I. Mareels, and B. Maschke, "Putting energy back in control," *IEEE Control Syst. Mag.*, vol. 21, no. 2, pp. 18–33, Apr. 2001.

[6] A. van der Schaft, *L_2-Gain and Passivity Techniques in Nonlinear Control*, 2nd ed. London, U.K.: Springer-Verlag, 2000.

[7] D. Wang and N. McClamroch, "Position and force control for constrained manipulator motion: Lyapunov's direct method," *IEEE Trans. Robot. Autom.*, vol. 9, no. 3, pp. 308–313, Jun. 1993.

[8] V. Parra-Vega and S. Arimoto, "A passivity-based adaptive sliding mode position-force control for robot manipulators," *Int. J. Adapt. Control Signal Process.*, vol. 10, pp. 365–377, Jul. 1996.

[9] L. Whitcomb, S. Arimoto, T. Naniwa, and F. Ozaki, "Adaptive model-based hybrid control of geometrically constrained robot arms," *IEEE Trans. Robot. Autom.*, vol. 13, no. 1, pp. 105–116, Feb. 1997.

[10] J. Roy and L. Whitcomb, "Adaptive force control of position/velocity controlled robots: Theory and experiment," *IEEE Trans. Robot. Autom.*, vol. 18, no. 2, pp. 121–137, Apr. 2002.

[11] C. Chiu, K. Lian, and T. Wu, "Robust adaptive motion/force tracking control design for uncertain constrained robot manipulators," *Automatica*, vol. 40, no. 12, pp. 2111–2119, Dec. 2004.

[12] J.-J. Slotine and W. Li, "Adaptive strategies in constrained manipulation," in *Proc. IEEE Int. Conf. Robot. Autom.*, vol. 4. Mar. 1987, pp. 595–601.

[13] J. Wen and S. Murphy, "Stability analysis of position and force control for robot arms," *IEEE Trans. Autom. Control*, vol. 36, no. 3, pp. 365–371, Mar. 1991.

[14] S. Chiaverini, B. Siciliano, and L. Villani, "Force/position regulation of compliant robot manipulators," *IEEE Trans. Autom. Control*, vol. 39, no. 3, pp. 647–652, Mar. 1994.

[15] Z. Doulgeri and Y. Karayiannidis, "Performance analysis of a soft tip robotic finger controlled by a parallel force/position regulator under kinematic uncertainties," *IET Control Theory Appl.*, vol. 1, no. 1, pp. 273–280, Jan. 2007.

[16] Z. Doulgeri and Y. Karayiannidis, "Force position control for a robot finger with a soft tip and kinematic uncertainties," *Robot. Autom. Syst.*, vol. 55, no. 4, pp. 328–336, Apr. 2007.

[17] S. Arimoto, H. Han, C. Cheah, and S. Kawamura, "Extension of impedance matching to nonlinear dynamics of robotic tasks," *Syst. Control Lett.*, vol. 36, no. 2, pp. 109–119, Feb. 1999.

[18] N. Hogan, "Impedance control: An approach to manipulation: Parts I–III," *ASME J. Dyn. Sys., Meas., Control*, vol. 107, pp. 1–24, Mar. 1985.

[19] A. Donaire and S. Junco, "On the addition of integral action to port-controlled Hamiltonian systems," *Automatica*, vol. 45, no. 8, pp. 1910–1916, Aug. 2009.

[20] R. Ortega and J. G. Romero, "Robust integral control of port-hamiltonian systems: The case of non-passive outputs with unmatched disturbances," *Syst. Control Lett.*, vol. 61, pp. 11–17, Jan. 2012.

[21] J. G. Romero, A. Donaire, and R. Ortega, "Robust energy shaping control of mechanical systems," *Syst. Control Lett.*, vol. 62, no. 9, pp. 770–780, Sep. 2013.

[22] K. Fujimoto, K. Sakurama, and T. Sugie, "Trajectory tracking control of port-controlled Hamiltonian systems via generalized canonical transformations," *Automatica*, vol. 39, no. 12, pp. 2059–2069, Dec. 2003.

[23] D. Navarro-Alarcon, P. Li, and H. M. Yip, "Energy shaping control for robot manipulators in explicit force regulation tasks with elastic environments," in *Proc. IEEE Int. Conf. Intell. Robot. Syst.*, Sep. 2011, pp. 4222–4228.

[24] M. H. Raibert and J. J. Craig, "Hybrid position/force control of manipulators," *ASME J. Dyn. Sys., Meas., Control*, vol. 103, no. 2, pp. 126–133, Jun. 1981.

[25] K. Fujimoto and T. Sugie, "Canonical transformation and stabilization of generalized Hamiltonian systems," in *Proc. 4th IFAC Symp. Nonlinear Control Syst. Des.*, 1998, pp. 544–549.

[26] S. Arimoto, *Control Theory of Non-linear Mechanical Systems: A Passivity-Based and Circuit-Theoretic Approach*. New York, NY, USA: Oxford Univ. Press, 1996.

[27] R. Ortega, J. Loria Perez, P. Nicklasson, and H. Sira-Ramirez, *Passivity-based Control of Euler-Lagrange Systems*, 1st ed. New York, NY, USA: Springer-Verlag, 1998.

[28] R. Ortega, A. J. van der Schaft, B. Maschke, and G. Escobar, "Interconnection and damping assignment passivity-based control of port-controlled Hamiltonian systems," *Automatica*, vol. 38, no. 4, pp. 585–596, Apr. 2002.

[29] R. Volpe and P. Khosla, "A theoretical and experimental investigation of explicit force control strategies for manipulators," *IEEE Trans. Autom. Control*, vol. 38, no. 11, pp. 1634–1650, Nov. 1993.

[30] A. Venkatraman, R. Ortega, I. Sarras, and A. van der Schaft, "Speed observation and position feedback stabilization of partially linearizable mechanical systems," *IEEE Trans. Autom. Control*, vol. 55, no. 5, pp. 1059–1074, May 2010.

[31] J. Slotine and W. Li, "On the adaptive control of robot manipulators," *Int. J. Robot. Res.*, vol. 6, no. 3, pp. 49–59, Sep. 1987.

[32] D. Jeltsema and J. Scherpen, "Multidomain modeling of nonlinear networks and systems," *IEEE Control Syst. Mag.*, vol. 29, no. 4, pp. 28–59, Aug. 2009.

[33] M. Vidyasagar, *Nonlinear Systems Analysis*, 2nd ed. Englewood Cliffs, NJ, USA: Prentice-Hall, 1993.

[34] J. G. Romero, D. Navarro-Alarcon, and E. Panteley, "Robust globally exponentially stable control for mechanical systems in free/constrained-motion tasks," in *Proc. IEEE Conf. Decision Control*, Jan. 2013, pp. 3067–3072.

[35] E. D. Sontag, "Input to state stability: Basic concepts and results," in *Nonlinear and Optimal Control Theory*, P. Nistri and G. Stefani, Eds. New York, NY, USA: Springer-Verlag, 2006, pp. 163–220.

[36] F. Pertin and J.-M. Bonnet des Tuves, "Real time robot controller abstraction layer," in *Proc. Int. Symp. Robot.*, Mar. 2004, p. 71.

[37] P. Gerum, *Xenomai—Implementing a RTOS Emulation Framework on GNU/Linux*, 1st ed. New York, NY, USA: Wiley, Apr. 2004.

[38] M. Galassi *et al.*, *GNU Scientific Library Reference Manual*, 3rd ed. Godalming, U.K.: Network Theory Ltd., 2009.

[39] D. Navarro-Alarcon, Y.-H. Liu, J. G. Romero, and P. Li, "Model-free visually servoed deformation control of elastic objects by robot manipulators," *IEEE Trans. Robot.*, vol. 26, no. 6, pp. 1457–1468, Aug. 2013.

[40] D. Navarro-Alarcon and Y.-H. Liu, "Uncalibrated vision-based deformation control of compliant objects with online estimation of the Jacobian matrix," in *Proc. IEEE Int. Conf. Intell. Robot. Syst.*, Jan. 2013, pp. 4977–4982.